RSC Advances

PAPER

View Article Online
View Journal | View Issue

Cite this: *RSC Adv.*, 2023, **13**, 594

Luminescent 1*H*-1,3-benzazaphospholes†

Sloane Evariste, [a] Alexandra M. Harrison, [a] Sunandan Sarkar,[b] Arnold L. Rheingold, [c] Barry D. Dunietz, [d] Joachim W. Heinicke, [e] Emalyn Delgado Rosario, [a] Sungwoon Yoon, [f] Thomas S. Teets [f] and John D. Protasiewicz *[a]

Received 14th November 2022
Accepted 14th December 2022

DOI: 10.1039/d2ra07226b

rsc.li/rsc-advances

2-R-1*H*-1,3-Benzazaphospholes (**R-BAP**s) are an interesting class of σ^2P heterocycles containing P=C bonds. While closely related 2-R-1,3-benzoxaphospholes (**R-BOP**s) have been shown to be highly photoluminescent materials depending on specific R substituents, photoluminescence of **R-BAP**s has been previously limited to an example having a fused carbazole ring system. Here we detail the synthesis and structural characterization of a new **R-BAP** (**3c**, R = 2,2′-dithiophene), and compare its photoluminescence against two previously reported **R-BAP**s (**3a**, R, R′ = Me and **3b**, R = 2-thiophene). The significant fluorescence displayed by the thiophene derivatives **3b** (φ = 0.53) and **3c** (φ = 0.12) stands in contrast to the weakly emissive methyl substituted analogue **3a** (φ = 0.08). Comparative computational investigations of **3a–c** offer insights into the interplay between structure–function relationships affecting excited state relaxation processes.

Introduction

Organic π-conjugated materials continue to receive widespread attention; their optical and electronic properties make them potential candidates as semiconducting materials in optoelectronic devices.[1–12] Many different strategies are being used to improve or modulate the electronic properties of π-conjugated oligomers or polymers, including incorporation of heterocyclopentadienes (such as thiophenes, pyrroles, and phospholes).[13–17]

Phosphorus containing heterocycles can be subdivided by coordination number, with three coordinate and four coordinate geometries (σ^3, σ^4) being the most commonly studied systems.[18–24] In particular, σ^3,λ^3-phospholes have drawn much attention, as their (i) trigonal pyramidal geometry and reduced aromaticity allow for unusual means to tune electronic delocalization into the π-system, and (ii) the lone pair on phosphorus offers additional opportunities to modulate HOMO and LUMO levels. Specifically, chemical modification of the P atom by oxidation, alkylation, or coordination by Lewis acids and metals has led to tunable new π-conjugated systems with diverse photophysical properties.[25]

In particular, σ^4,λ^5-phospholes can display impressive luminescence, and many different types of derivatives have been synthesized for diverse potential applications (Chart 1, **A–D**).[26–35] For example, dibenzophospholes (**A**) have been used for OLEDs[36] and dithienophosphole building blocks (**B**) have been used to generate white light emission.[37] Fluorescent 2,2′-benzo[*b*]phosphole-benzo[*b*]heteroles (**C**)[38] and superphotostable dyes based on naphthalene-fused phospholes (**D**)[39] represent significant advances as well.

From this aspect, σ^2,λ^3-phospholes are much less studied. Such compounds feature PC pπ–pπ bonds directly analogous to conventional CC π bonds and offer further opportunities to explore π-conjugated materials. Our group has thus been interested in the development of luminescent phosphaalkenes featuring two-coordinate phosphorus atoms (σ^2).[40] In 2010,[41] we reported investigations of highly luminescent 1,3-benzoxaphospholes (**R-BOP**, Chart 1), and have since documented other luminescent benzoxaphosphole based materials.[42–46] The analogous sulfur-containing 1,3-benzothiaphospholes (**E**) are also luminescent.[47] While numerous 1*H*-1,3-benzazaphospholes (**R-BAP**) have been reported, no significant photoluminescence studies have appeared.[48–55] However, we have shown that a benzazaphosphole (**F**, Chart 1) adhered to carbazole (a common fluorophore) can display significant

[a]*Department of Chemistry, Case Western Reserve University, Cleveland, Ohio 44106, USA. E-mail: protasiewicz@case.edu*

[b]*Department of Chemistry, National Institute of Technology Tiruchirappalli, Tiruchirappalli, Tamil Nadu 620015, India*

[c]*Department of Chemistry and Biochemistry, University of California, La Jolla, San Diego, California 92093, USA*

[d]*Department of Chemistry and Biochemistry, Kent State University, Kent, Ohio 44242, USA*

[e]*Institut für Biochemie, Anorganische Chemie, Ernst-Moritz-Arndt-Universität Greifswald, Felix-Hausdorff-Str. 4, D-17489, Greisfwald, Germany*

[f]*Department of Chemistry, University of Houston, 3585 Cullen Blvd. Room 112, Houston, TX 77204-5003, USA*

† Electronic supplementary information (ESI) available: NMR spectra for compound **3c** and X-ray analysis data (table and CIF files) for compound **3c**. CCDC 2126128. For ESI and crystallographic data in CIF or other electronic format see DOI: **https://doi.org/10.1039/d2ra07226b**

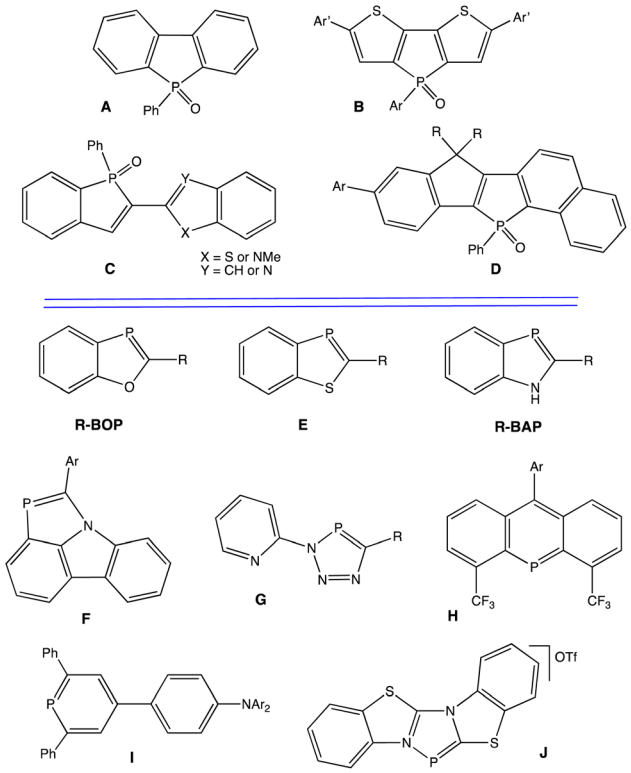

Chart 1 Examples of luminescent phospholes.

luminescence distinct from carbazole.[56] The development of other luminescent materials featuring σ^2,λ^3-phosphorus is rapidly expanding, as recent examples **G–J** illustrate in Chart 1.[57]

These observations inspired re-examination of selected **R-BAP**s to probe their potential as luminescent materials. In this study previously reported 2-thiophene-1,3-benzazaphosphole[58a] is shown to be highly luminescent. Comparisons are also made to a previously reported 2-methyl substituted analogue,[58b] as well as to a new 2-dithiophene analogue. Modifications of the 2-substituent are shown to lead to significant changes in emission properties, and the underlying photophysical reasons for these changes have been analyzed by computational studies.

Results and discussion

1*H*-1,3-Benzazaphospholes **3a–c** were identified for this study (Scheme 1). Compounds **3a** and **3b** were synthesized as previously reported.[58] Following similar protocols, the new BAP derivative **3c** was also prepared. The structure of **3c** was readily confirmed by routine NMR spectroscopic analyses. For example, the $^{31}P\{^1H\}$ NMR resonance for **3c** at δ 77.7 ppm is consistent with previously reported shifts for 1,3-benzazaphospholes, which typically range from δ 72.0 to 78.8 ppm.[58] Absolute identification of **3c** was made by an X-ray diffraction study.

Crystals of **3c** suitable for X-ray diffraction studies were grown by diffusion of pentane into a concentrated CH_2Cl_2 solutions of **3c**. The resulting solid-state structure is portrayed in Fig. 1, along with key bond lengths and angles (see ESI† for experimental details).

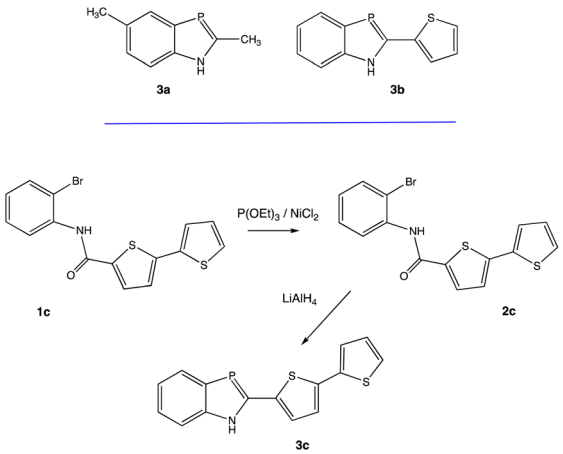

Scheme 1 1*H*-1,3-benzazaphospholes **3a** and **3b** (top), preparation of **3c** (bottom).

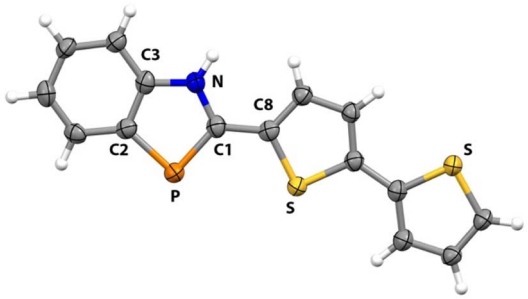

Fig. 1 X-ray crystal structure of compound **3c**. Selected bond lengths (Å) and bond angles (°) of **3c**: P═C_1 1.745(5), P–C_2 1.800(5), N–C_1 1.353(7), N–C_3 1.381(6), C_2–C_3 1.395(7), C_1–C_8 1.449(8), C_1–P–C_2 88.8(2), N–C_1–P 113.1(4), C_1–N–C_3 114.8(4).

The P═C1 bond length in **3c** (1.745(5) Å) is slightly longer than those distances found in related BAP derivatives (1.70–1.73 Å range).[58,59] This value is between single and double bonds owing to delocalization across the NCP array. The C_1–P–C_2 angle in **3c** (88.8(2)°) is consistent with such angles determined in related BAPs (88.2–90.1° range). Consistent with this hypothesis, all of the atoms in **3c** lie in a nearly perfect plane (max deviation from mean plane is 0.16 Å for remote S atom).

The crystal packing diagram for compound **3c** is represented in Fig. 2, and no π–π stacking interactions are noted in the crystalline state. Instead, a herringbone head-to-tail

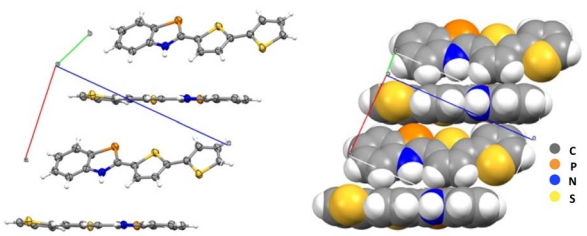

Fig. 2 Packing diagrams for derivative **3c**.

configuration along the a-axis (closest CH···centroid distance 3.0 Å) is observed. The centroid distance between two phosphole rings was found to be *ca.* 4.42 Å for **3c**, which is larger than π–π interactions observed for some other BAP derivatives (*ca.* 3.45 Å).

Optical properties of BAP derivatives

The UV/Vis absorption and fluorescence spectra of the three compounds **3a–c** were recorded in dry degassed CH_2Cl_2 (Table 1). All three BAP derivatives exhibit an absorption maximum in the UV-visible region (Fig. 3), attributed to π–π* transitions in the extended π-conjugated system. The nature of the substituent has a noticeable influence on the absorption maximum (λ_{max}(**3a**) = 297 nm < λ_{max}(**3b**) = 335 nm < λ_{max}(**3c**) = 398 nm; Table 1), revealing enhanced π-conjugation that leads to the absorption wavelength being red-shifted. Thus, the extended system **3c** possessing two thiophene rings absorbs at the longest wavelengths and across a wider UV-visible region compared to the others.

On excitation at λ_{max}, all the derivatives **3a–c** emit in the visible region (Fig. 4). The same trend was observed with a red-shift in the emission spectra when the 2-R substituent is aromatic (λ_{em}(**3b**) = 470 nm), rather than being aliphatic (λ_{em}(**3a**) = 407 nm). The addition of a second thiophene to the first shifts the emission maximum further (λ_{em}(**3c**) = 508 nm), evidence that the π-conjugation is extended through the terminal thiophene ring. The reasons for the presence of a small shoulder for the emission for **3a** are unclear, but it is unlikely to be due to aggregation. The fluorescence quantum yields ϕ_F in solution vary from 8% for **3a** (2-R = CH_3) to 53% for **3b** (2-R = 2-thiophene). The quantum yield of **3c** drops (ϕ_F = 12%) compared to the **3b** derivative possessing only one thiophene unit. The emission maxima from **3a** to **3b** are also similar to luminescent benzoxaphospholes.[41] The photophysics of the direct phosphorus-free (isolobal replacement of P for CH unit) indole analogue of **3b** (**THOIN**, Chart 2) has been examined experimentally and theoretically in some detail.[60]

Table 1 Experimental UV-visible and fluorescence data[a]

	λ_{max} (nm)	log ε	$\lambda_{F,max}$ (nm)	ϕ_F
3a	297	3.81	407	0.08[b]
3b	335	4.14	470	0.53[c]
3c	398	4.30	508	0.12[d]
THOIN[e]	317	—	379	0.22

[a] All measurements were performed in CH_2Cl_2. [b] Fluorescence quantum yield determined relative to 9,10-diphenylanthracene in cyclohexane. [c] Fluorescence quantum yield determined relative to anthracene in ethanol. [d] Fluorescence quantum yield determined relative to quinine sulfate in 0.5 M H_2SO_4 solution. [e] Data from ref. 60, *n*-hexane solvent.

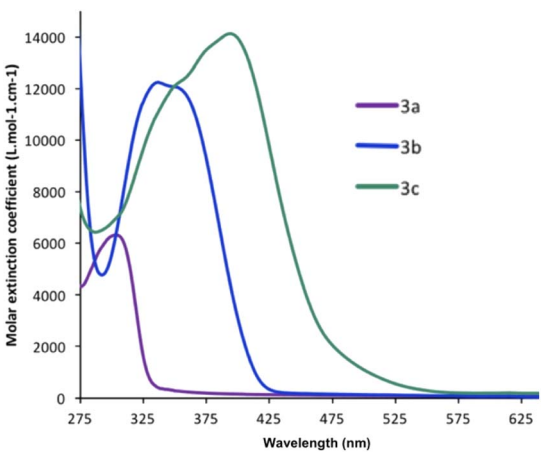

Fig. 3 Absorption spectra recorded in CH_2Cl_2 for compounds **3a–c**.

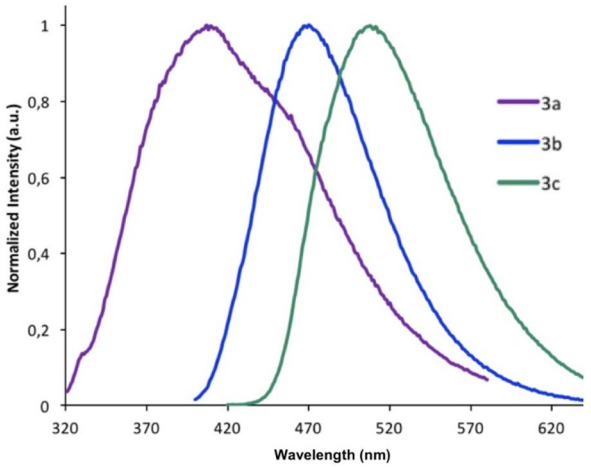

Fig. 4 Emission spectra recorded in CH_2Cl_2 for compounds **3a–c**. Each derivative was excited at its maximal absorbance λ_{max}.

The absorption maximum for compound **3b** is red shifted compared to **THOIN** (Table 1) by 18 nm. The emission maxima, however, is shifted by 91 nm, yielding a significant Stokes shift of 135 nm (stokes shifts: **THOIN**: 5150 cm^{-1}; **3b**: 8574 cm^{-1}; **3c**: 5441 cm^{-1}). Stokes shifts for Ar-BOPs range from 79 to 89 nm (5401–5852 cm^{-1}). Thiophene substituted heterocycles such as **BBT-R** (Chart 2, R = NH_2) have been developed showing even larger Stokes shifts, up to 186 nm (8752 cm^{-1}).[61,62] Large Stokes shifts have been associated with various features, such as intramolecular charge transfer (ICT), rotation of π-conjugated substituents, excited state intramolecular proton transfer (ESIPT) processes, and solvent effects.[63] The larger Stokes shift observed for **3b** might reflect significant changes in bond lengths upon excitation (*vide infra*).

Both absorption and emission spectra of compound **3b** were recorded in several solvents (toluene, THF, dichloromethane,

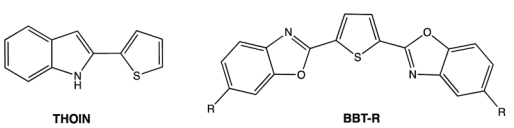

Chart 2 Related luminescent molecules.

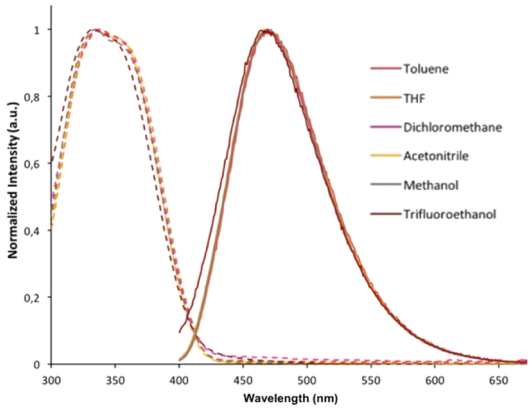

Fig. 5 Absorption (dotted lines) and emission spectra (solid lines; λ_{exc} = 320 nm) for compound **3b** recorded in different polarity solvents.

acetonitrile, methanol and trifluoroethanol; Fig. 5). Regardless of the solvent, there was no significant modification in its optical properties, suggesting that the absorption and emission processes for **3b** do not involve significant charge transfer or special solvation effects. Indole derivative **THOIN** and Ar-BOPs also display solvent independent absorption and emission properties. Lifetime measurements conducted on **3b** and **3c** in CH_2Cl_2 revealed τ = 7.4 and 1.7 ns, respectively, which can be compared to fluorescence lifetimes determined for Ar-BOP (τ = 4.8–28.0)[41] and **THOIN** (τ = 0.8).[60]

Computational studies

Density functional theory (DFT) and time-dependent DFT (ωB97X-D/6-311++G(d,p) in polarizable continuum model (PCM)) calculations were employed to study the materials at the electronic structure level. The calculated ground state structural parameters (bond lengths and angles) for **3a** and **3c** correspond well with corresponding measured values from X-ray structure analyses. As shown in Table 2, the calculated bond lengths are within 0.15 Å of the measured data, and the calculated bond angles are within one degree of measured values.

With the calculated geometries in excellent agreement with the crystallographic results, we proceeded to consider the excited states. Our approach follows our previous study on related organophosphorus systems[64–67] and uses well benchmarked methods.[64–66] The $S_0 \rightarrow S_1$ excitations of **3a–c** mainly correspond to the HOMO → LUMO transitions. The electronic densities associated with the HOMO and LUMO are delocalized throughout the π-systems for all compounds. In both **3b** and **3c** the π-conjugation is extended across the molecule including the thiophene unit. Hence, a decrease in the HOMO–LUMO energy gap is observed with the increase of the π-conjugation in the series (ΔE_g(**3a**) = 8.32 eV > ΔE_g(**3b**) = 7.35 eV > ΔE_g(**3c**) = 7.08 eV; Fig. 6). As a result, the calculated lowest energy state (S_1) is shifted towards longer wavelengths from **3a** to **3c** for both the absorption and emission processes (Table 3).

Upon excitation, longer P=C bond lengths for **3b** (*Δ* 0.112 Å) and **3c** (*Δ* 0.074 Å) are predicted (see Fig. S5 in ESI† for mapping of other bond length changes). The greater change in PC bond length for **3b** correlates with this material showing an enhanced Stokes shift. The CC bond bridging the BAP and directly connected thiophene shows corresponding bond length decreases (*ca.* 0.07 Å), which are consistent with the tendency of these systems to planarize in the excited state.

The alkyl substituted derivative displays significantly lower quantum yield for emission than found for the thiophene derivatives. Part of this can be attributed to the reduced oscillator strength *f* (0.21, Table 3) for the emission state of **3a**, relative to those calculated for **3b** (0.60) and **3c** (1.00). If reduced oscillator strengths were the sole determining factor in controlling quantum yields, the quantum yield for **3c** should be greater than that for **3b**. However, **3b** has greater than four times higher quantum yield than that associated with **3c**. To explain this seeming contradiction, we need to explore also competing thermal non-radiative processes from the lowest lying excited states. Recently we analyzed computationally the relationships of structure and fluorescence yields in **R-BOP**s and **R-BAPs**.[64] The intensity of fluorescence emission is dependent on the nature of the R substituent (alkyl < aryl) and the ability of the system to adopt a planar geometry in the excited state. Compared to **R-BOP**s, Ar-BAPs with potential N(R′)···H–Ar steric clashes can lead to deflection of the attached six- and five-membered rings from optimal geometry for π-conjugation and reduced photoluminescence. Steric clashes between two

Table 2 Select computed key bond lengths (Å) and bond angles (°) for R-BAP (experimental values from X-ray data in parenthesis)

Parameters	**3a** (ref. 58*b*)	**3b**	**3c**
P–C1	1.728 (1.728)	1.734	1.733 (1.745)
P–C2	1.799 (1.793)	1.791	1.791 (1.800)
N–C1	1.355 (1.369)	1.359	1.360 (1.353)
N–C3	1.379 (1.380)	1.373	1.373 (1.381)
C2–C3	1.407 (1.413)	1.408	1.408 (1.395)
C1–C8	1.495 (1.493)	1.457	1.457 (1.449)
C1–P–C2	89.1 (89.5)	88.8	88.7 (88.8)
N–C1–P	113.5 (113.3)	113.5	113.6 (113.1)
C1–N–C3	115.0 (114.6)	114.7	114.6 (114.8)

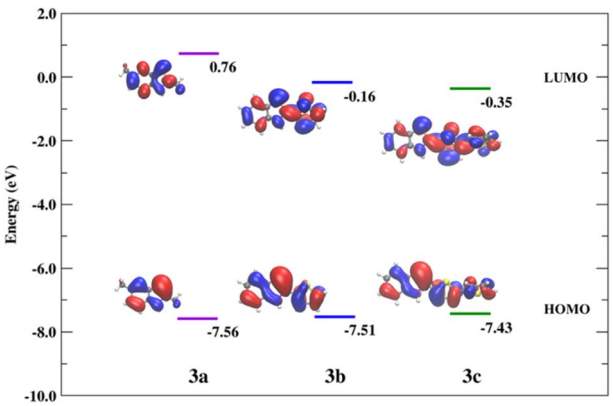

Fig. 6 Spatial plots of the HOMO and LUMO of **3a–c**.

Table 3 Comparison of experimental and calculated optical data

	λ_{max} exp (nm)	λ_{max} calc (nm)	F (H → L)	λ_{em} exp (nm)	λ_{em} calc (nm)	F (H ← L)
3a	297	263	0.209 (0.94)	407	302	0.198 (0.93)
3b	335	319	0.602 (0.96)	470	404	0.597 (0.97)
3c	398	336	1.005 (0.95)	508	464	1.118 (0.97)

attached five-membered heterocyclic rings, however, are expected to be less severe. This expectation is supported by the observed planar X-ray structure of **3c**. While this explanation alone may partly account for why compound **3b** (Th-BAP) is luminescent and other BAPs have not been reported to be emissive, it does not explain why **3b** is much more emissive than **3c**.

Our working model involves comparing the calculated rates of fluorescence (k_{fl}) and intersystem crossing (k_{isc}) from the first excited state (S_1). Effective emission must compete with non-radiative decay (k_{nrd}, thermal relaxation). Rigid ring systems can help minimize k_{nrd} relative to k_{fl}. If, however, efficient conversion to nearby triplet states can occur, these longer lived states give more time for k_{nrd} to compete and reduce emission (Fig. 7). In most non-transition-metal compounds room temperature phosphorescence does not compete with non-radiative decay except in special situations or in the solid state.[68] **BBT-R** (R = ^{t}Bu), for example, has been shown to undergo competitive fluorescence quenching by intersystem crossover to nearby triplet state.[61,62] This view is supported by the facts that (a) we have not observed lower wavelength (up to 800 nm) emissions attributable to phosphorescence in **R-BOP**s or **R-BAP**s, (b) emission spectra for both sets of compounds are similar, (c) lifetime measurements for **3b** and **3c** are consistent with fluorescence (neither of these compounds display visible luminescence under UV-light in the solid state), and (d) the predicted λ_{em} correlate with experimental data.

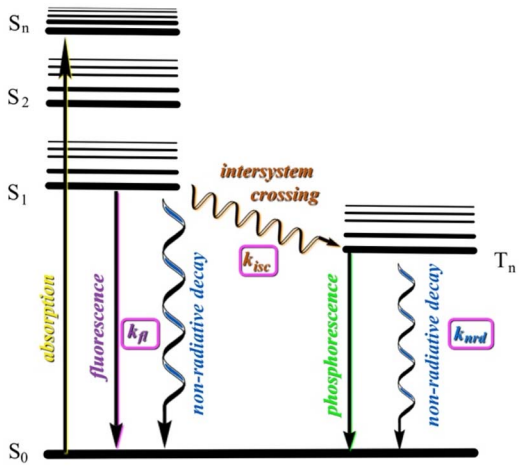

Fig. 7 Jablonski diagram showing key events after absorption and internal conversion (not shown) to S_1 excited state. Wavy lines represent non-radiative processes.

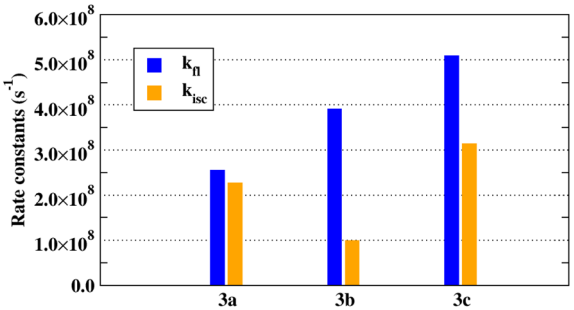

Fig. 8 Radiative and non-radiative rate constants for **3a–c**.

Indeed, we found that higher fluorescence quantum yields are also associated with higher ratios of $k_{fl}:k_{isc}$. Radiative (fluorescence, blue bars) and non-radiative (intersystem crossing, orange bars) calculated rate constants of **3a–c** are represented in Fig. 8. The fluorescence rates increase with the extension of the conjugation system, following the expected increasing trend with the oscillator strength of the emitting state (Table 3). The competing ISC non-radiative relaxation is the smallest for **3b**. The ratio $k_{fl}:k_{isc}$ is the largest for **3b**, where it is less than two for **3c** and close to one for **3a**. This prediction is consistent with the experimental observation that **3b** has the highest FL quantum yield.

To understand the trend of the ISC rates, the semiclassical Marcus theory of activated transition states was used as employed in our studies of related systems.[64–66] The calculated parameters along with the rate constants are listed in Table 4. The processes are not in the far-inverted regime (comparing the energy bias [ΔG] to the reorganization energy [E_r]), validating the semiclassical limit. In all cases the singlet-triplet spin–orbit coupling (SOC) is weak since all the states are of the same state character (π–π^*). Nevertheless, the resulting intersystem crossing rate constants remain significant when compared to the fluorescence rate constants.

The activation energy (E_a) for the singlet-triplet transition is low, while the energy for **3b** is relatively the highest of the considered systems (Table 4). In case of **3b**, the triplet excited state is ~110 meV higher than the singlet excited state at lowest

Table 4 Calculated data for singlet-triplet intersystem crossing

	SOC (cm^{-1})	ΔG (eV)	E_r (eV)	E_a (eV)	k_{isc} (s^{-1})
3a	0.92	−0.858	0.901	5.15×10^{-4}	2.27×10^8 (S_1–T_3)
3b	0.55	−0.113	0.222	1.33×10^{-2}	0.99×10^8 (S_1–T_2)
3c	0.74	−0.214	0.178	1.76×10^{-3}	3.13×10^8 (S_1–T_2)

singlet excited state minima. These singlet-triplet splitting at lowest singlet excited state minima are smaller (around ± 30–40 meV) for the other two systems. This trend of singlet-triplet splitting energy leads to the higher ratio of reorganization (E_r) to free energy (ΔG) for **3b** and therefore to increase the activation energy, resulting with the lowest ISC rate.

Experimental

General materials and methods

All reactions were performed under an atmosphere of rigorously dry and oxygen-free nitrogen using either a MBraun Labmaster 130 glove box or standard Schlenk line techniques. Unless otherwise stated, all chemicals were purchased from commercial sources and used without further purification. Dry diethyl ether and hexanes were obtained from a MBraun SPS-800 solvent drying and purification system using filter material MB-KOL-A. The intermediate compounds *N*-(2-bromophenyl)-[2,2′-dithiophene]-5-carboxamide (**1c**) and {2-[((2,2′-dithiophene)-5-carbonyl)amino]phenyl} phosphonic acid diethyl ester (**2c**) were prepared according to literature procedures reported previously.[58]

Dichloromethane-d_2 was dried over basic alumina and degassed prior to use. NMR spectra were recorded on a Bruker Ascend Advanced III HD NMR spectrometer operating at 500.24 MHz and 202.5 MHz for ^{1}H and ^{31}P{^{1}H} NMR, respectively. ^{31}P{^{1}H} NMR were referenced to 85% H_3PO_4. Dichloromethane was dried by distillation from calcium hydride prior to use for UV/Vis and fluorescence measurements. UV/Vis data were recorded by using a Cary 50 Bio UV/Vis spectrophotometer. Molar absorptivity determination was verified by linear least-squares fit of values obtained from at least three independent solutions at varying concentrations with absorbance in the range of 10^{-5} M. Emission spectra were recorded by using a Cary Eclipse spectrometer. The samples were excited at their absorption maximum. Emission quantum yields were determined by using as standards 9,10-diphenylanthracene in cyclohexane for compound **3a**, anthracene in ethanol for **3b** and quinine sulfate in 0.5 M H_2SO_4 solution for **3c**, respectively (conc. 10^{-6} M). The excitation slit width for all measurements was kept at default settings (5 nm).

X-ray crystallography

Data were collected at 100K. The supplementary crystallographic data for **3c** (CCDC 2126128). Tables S1–S5† contain selected data collection and refinement details-results. Fig. S3† offers a detailed packing diagram for **3c**.

Computational

The DFT calculations were implemented using Q-Chem as described in ESI.†

Synthesis of 2-([2,2′-dithiophen]-5-yl)-1*H*-1,3-benzazaphosphole (3c). Compound **2c** (0.543 g, 1.29 mmol) dissolved in diethyl ether (5 mL) and THF (2 mL) was added dropwise at 0 °C to $LiAlH_4$ (0.147 mg, 3.87 mmol) stirred in diethyl ether (5 mL). After stirring at 40 °C overnight, the mixture was hydrolyzed at 0 °C. The insoluble solid was filtered off under nitrogen and thoroughly washed with diethyl ether. The filtrate was dried over Na_2SO_4, transferred into another flask and the solvent removed in vacuum. The product was then purified by column chromatography on silica gel under nitrogen, using hexanes-diethyl ether as eluents and recrystallized with hexanes. Yield: 0.049 g (13%). ^{31}P{^{1}H} NMR (CD_2Cl_2): δ 77.7. ^{1}H NMR (CD_2Cl_2): δ 9.37 (s, 1H), 8.00 (dd, J = 7.9, 3.8 Hz, 1H), 7.62 (d, J = 8.1 Hz, 1H), 7.41–7.34 (m, 2H), 7.30 (d, J = 5.1 Hz, 1H), 7.27 (d, J = 3.4 Hz, 1H), 7.22–7.19 (m, 1H), 7.16 (t, J = 7.3 Hz, 1H), 7.09–7.05 (m, 1H). ^{13}C{^{1}H} NMR (126 MHz, CD_2Cl_2): δ 166.3 (d, J = 48.3 Hz), 142.5 (d, J = 7.08 Hz), 141.4 (d, J = 41.7 Hz), 137.5 (d, J = 6.41 Hz), 136.8 (d, J = 18.8 Hz), 136.6, 128.5 (d, J = 20.5 Hz), 128.0, 125.6 (d, J = 3.11 Hz), 125.1, 124.6, 124.2, 124.0 (d, J = 12.7 Hz), 120.7 (d, J = 12.6 Hz), 113.4. HRMS (EI): calcd. for **3c**: 298.9992; found: 298.9987.

Conclusions

1*H*-1,3-Benzazaphospholes (**R-BAP**s) are very well known materials with well-developed synthesis and applications, yet no photophysical studies have been reported despite close analogies to the related class of compounds 1,3-benzoxaphospholes (**R-BOP**s). In this work, we have demonstrated that selected **R-BAP**s can indeed display significant photoluminescence. The presence of one thiophene substituent (**3b**) or two (**3c**) leads to a better electron delocalization of the π-conjugated system and longer λ_{max} values for absorption compared to the methyl-substituted compound (**3a**). X-ray diffraction studies show that the BAP ring and the connecting di-thiophene rings are highly coplanar in the solid state, also suggesting high degree of π-conjugation. The emission properties of **3c** are also red-shifted towards the longest wavelengths compared to the others. TD-DFT calculations confirm the presence of π-conjugation throughout the BAP system. Computational efforts also revealed several factors that give rise to effective photoluminescence from **R-BAP**s. First, the presence of 5-membered thiophene units at the 2-position of the BAP group allows for easier adoption of an emissive planar configuration. Second, high oscillator strengths needed for emission are indicated. Third, the relative rates of fluorescence to intersystem crossing (a non-radiative decay pathway) are most favorable for compound **3b**. Overall, this work provides a molecular understanding for means to develop **BAP**-based materials for optimal use in optoelectronic applications.

Author contributions

JDP conceptualized the project. SE, AMH, and EDR carried out synthesis and spectral characterization of compounds. TST and SY measured excited state lifetimes. JH provided an initial sample of compound **3a**, and intellectual guidance. BDD and SS performed all computational studies and provided interpretation of data. ALR conducted the crystallographic studies. All authors helped to write and to proofread manuscript.

Conflicts of interest

The authors declare no conflicts of interest.

Acknowledgements

J. D. Protasiewicz thanks the National Science Foundation (CHE-1464855 and CHE-1955845) for funding. B. D. Dunietz acknowledges the Department of Energy (DOE), Basic Energy Sciences through Grant No. DE-SC0016501. We are also grateful to the college of Arts and Sciences, Kent State University for computing resources. T. S. Teets thanks the National Science Foundation (CHE-1846831) for support. We also thank Professor Zacharias Kinney (Oakland University) and reviewers for helpful comments.

References

1 J. R. Sheats and P. F. Barbara, *Acc. Chem. Res.*, 1999, **32**, 191–192.
2 J. L. Segura and N. J. Martín, *Mater. Chem.*, 2000, **10**, 2403–2435.
3 H. Hoppe and N. S. Sariciftci, *J. Mater. Res.*, 2004, **19**, 1924–1945.
4 K. M. Coakley and M. D. McGehee, *Chem. Mater.*, 2004, **16**, 4533–4542.
5 A. P. Kulkarni, C. J. Tonzola, A. Babel and S. A. Jenekhe, *Chem. Mater.*, 2004, **16**, 4556–4573.
6 S. Günes, H. Neugebauer and N. S. Sariciftci, *Chem. Rev.*, 2007, **107**, 1324–1338.
7 S.-C. Lo and P. L. Burn, *Chem. Rev.*, 2007, **107**, 1097–1116.
8 G. Dennler, M. C. Scharber and C. J. Brabec, *Adv. Mater.*, 2009, **21**, 1323–1338.
9 (*a*) M. Helgesen, R. Søndergaard and F. C. Krebs, *J. Mater. Chem.*, 2010, **20**, 36; (*b*) A. Facchetti, *Chem. Mater.*, 2011, **23**, 733–758.
10 F. Riobe, R. Szűcs, P.-A. Bouit, D. Tondelier, B. Geffroy, F. Aparicio, J. Buendía, L. Sanchez, R. Reau, L. Nyulaszi and M. Hissler, *Chem.–Eur. J.*, 2015, **21**, 6547–6556.
11 M. P. Duffy, P.-A. Bouit, B. Geffroy, D. Tondelier and M. Hissler, *Phosphorus Sulfur Relat. Elem.*, 2016, **190**, 845–853.
12 D. Joly, P.-A. Bouit and M. Hissler, *J. Mater. Chem. C*, 2016, **4**, 3686–3698.
13 B. M. Wong and J. G. Cordaro, *J. Phys. Chem. C*, 2011, **115**, 18333–18341.
14 B. N. Norris, S. Zhang, C. M. Campbell, J. T. Auletta, P. Calvo-Marzal, G. R. Hutchison and T. Y. Meyer, *Macromolecules*, 2013, **46**, 1384–1392.
15 H. Sun and J. Autschbach, *J. Chem. Theory Comput.*, 2014, **10**, 1035–1047.
16 T. Körzdörfer and J.-L. Brédas, *Acc. Chem. Res.*, 2014, **47**, 3284–3291.
17 T. Fukushima, *Mater. Chem. Front.*, 2018, **2**, 1594.
18 F. Mathey, *Angew. Chem., Int. Ed. Engl.*, 2003, **42**, 1578–1604.
19 T. Baumgartner and R. Réau, *Chem. Rev.*, 2006, **106**, 4681–4727.
20 M. Hissler, P. W. Dyer and R. Réau, *Top. Curr. Chem.*, 2005, **250**, 127–163.
21 D. Joly, D. Tondelier, V. Deborde, B. Geffroy, M. Hissler and R. Réau, *New J. Chem.*, 2010, **34**, 1603–1611.
22 D. Joly, D. Tondelier, V. Deborde, W. Delaunay, A. Thomas, K. Bhanuprakash, B. Geffroy, M. Hissler and R. Réau, *Adv. Funct. Mater.*, 2012, **22**, 567–576.
23 J. Moon, M. Kim, J. S. Lim and J. Kim, *Mol. Phys.*, 2018, **116**, 1581–1588.
24 V. Iaroshenko and S. Mkrtchyan, *Organophosphorus Chemistry: From Molecules to Applications*, 2019, pp. 295–456.
25 M. P. Duffy, P.-A. Bouit and M. Hissler, in *Main Group Strategies towards Functional Hybrid Materials*, ed. T. Baumgartner and F. Jäkle, John Wiley & Sons Ltd., Hoboken, Chichester, 2018, ch. 12, pp. 295–327.
26 T. Baumgartner, *Acc. Chem. Res.*, 2014, **47**, 1613–1622.
27 M. A. Shameem and A. Orthaber, *Chem.–Eur. J.*, 2016, **22**, 10718–10735.
28 S. Yamaguchi, A. Fukazawa and M. Taki, *J. Synth. Org. Chem., Jpn.*, 2017, **75**, 1179–1187.
29 T. Higashino, K. Ishida, T. Sakurai, S. Seki, T. Konishi, K. Kamada, K. Kamada and H. Imahori, *Chem.–Eur. J.*, 2019, **25**, 6425–6438.
30 S. M. Parke, S. Tanaka, H. Yu, E. Hupf, M. J. Ferguson, Y. Zhou, K. Naka and E. Rivard, *Macromolecules*, 2019, **52**, 7477–7488.
31 C. Wang, M. Taki, K. Kajiwara, J. Wang and S. Yamaguchi, *ACS Mater. Lett.*, 2020, **2**, 705–711.
32 Y. Xu, R. Xu, Z. Wang, Y. Zhou, Q. Shen, W. Ji, D. Dang, L. Meng and B. Z. Tang, *Chem. Soc. Rev.*, 2021, **50**, 667–690.
33 S. Ikeda, A. Yoshimura, T. Shirahata, Y. Matano and Y. Misaki, *Chem. Lett.*, 2021, **50**, 1581–1585.
34 Y. Sugihara, N. Inai, M. Taki, T. Baumgartner, R. Kawakami, T. Saitou, T. Imamura, T. Yanai and S. Yamaguchi, *Chem. Sci.*, 2021, **12**, 6333–6341.
35 K. Ishida, T. Higashino, Y. Wada, H. Kaji, A. Saeki and H. Imahori, *ChemPlusChem*, 2021, **86**, 130–136.
36 H.-C. Su, O. Fadhel, C.-J. Yang, T.-Y. Cho, C. Fave, M. Hissler, C.-C. Wu and R. Réau, *J. Am. Chem. Soc.*, 2006, **128**, 983–995.
37 C. Romero-Nieto, S. Durben, I. M. Kormos and T. Baumgartner, *Adv. Funct. Mater.*, 2009, **19**, 3625–3631.
38 Y. Hayashi, Y. Matano, K. Suda, Y. Kimura, Y. Nakao and H. Imahori, *Chem.–Eur. J.*, 2012, **18**, 15972–15983.
39 C. Wang, M. Taki, Y. Sato, A. Fukazawa, T. Higashiyama and S. Yamaguchi, *J. Am. Chem. Soc.*, 2017, **139**, 10374–10381.
40 M. C. Simpson and J. D. Protasiewicz, *Pure Appl. Chem.*, 2013, **85**, 801–815.
41 M. P. Washington, V. B. Gudimetla, F. L. Laughlin, N. Deligonul, S. He, J. L. Payton, M. C. Simpson and J. D. Protasiewicz, *J. Am. Chem. Soc.*, 2010, **132**, 4566–4567.
42 F. L. Laughlin, A. L. Rheingold, N. Deligonul, B. J. Laughlin, R. C. Smith, L. J. Higham and J. D. Protasiewicz, *Dalton Trans.*, 2012, **41**, 12016–12022.
43 F. L. Laughlin, N. Deligonul, A. L. Rheingold, J. A. Golen, B. J. Laughlin, R. C. Smith and J. D. Protasiewicz, *Organometallics*, 2013, **32**, 7116–7121.

44 S. Wu, A. L. Rheingold and J. D. Protasiewicz, *Chem. Commun.*, 2014, **50**, 11036–11038.
45 A. B. Grimm, K. Wang, A. L. Rheingold, C. E. Moore, D. Szieberth, L. Nyulaszi and J. D. Protasiewicz, *Organometallics*, 2021, **40**, 3436–3444.
46 Z. T. Ekstrom, A. L. Rheingold and J. D. Protasiewicz, *Phosphorus, Sulfur Silicon Relat. Elem.*, 2021, **197**(5–6), 426–433.
47 (*a*) J. C. Worch, D. N. Chirdon, A. B. Maurer, Y. Qiu, S. J. Geib, S. Bernhard and K. J. T. Noonan, *J. Org. Chem.*, 2013, **78**, 7462–7469; (*b*) Y. Qiu, J. C. Worch, D. N. Chirdon, A. Kaur, A. B. Maurer, S. Amsterdam, C. R. Collins, T. Pintauer, D. Yaron, S. Bernhard and K. J. T. Noonan, *Chem.–Eur. J.*, 2014, **20**, 7746–7751.
48 J. Heinicke, N. Gupta, S. Singh, A. Surana, O. Kuhl, R. K. Bansal, K. Karaghiosoff and M. Vogt, *Z. Anorg. Allg. Chem.*, 2002, **628**, 2869–2876.
49 B. Niaz, M. Ghalib, P. G. Jones and J. Heinicke, *Dalton Trans.*, 2013, **42**, 9523–9532.
50 B. Niaz, F. Iftikhar, M. K. Kindermann, P. G. Jones and J. Heinicke, *Eur. J. Inorg. Chem.*, 2013, 4220–4227.
51 N. Gupta, C. B. Jain, J. Heinicke, R. K. Bansal and P. G. Jones, *Eur. J. Inorg. Chem.*, 1998, 1079–1086.
52 N. Gupta, C. B. Jain, J. Heinicke, N. Bharatiya, R. K. Bansal and P. G. Jones, *Heteroat. Chem.*, 1998, **9**, 333–339.
53 (*a*) G. Märkl and S. Pflaum, *Tetrahedron Lett.*, 1987, **28**, 1511–1514; (*b*) K. Issleib and R. Vollmer, *Z. Anorg. Allg. Chem.*, 1981, **481**, 22–32.
54 R. K. Bansal, N. Gupta, K. Karaghiosoff, A. Schmidpeter and C. Spindler, *Chem. Ber.*, 1991, **124**, 475–480.
55 (*a*) M. Ghalib, B. Niaz, P. G. Jones and J. W. Heinicke, *Tetrahedron Lett.*, 2012, **53**, 5012–5014; (*b*) B. R. Aluri, M. K. Kindermann, P. G. Jones and J. Heinicke, *Chem.–Eur. J.*, 2008, **14**, 4328–4335; (*c*) B. R. Aluri, P. G. Jones, I. Dix and J. W. Heinicke, *Synthesis*, 2014, **46**, 1773–1778; (*d*) J. Heinicke, K. Steinhauser, N. Peulecke, A. Spannenberg, P. Mayer and K. Karaghiosoff, *Organometallics*, 2002, **21**, 912–919; (*e*) A. Surana, S. Singh, R. K. Bansal, N. Peulecke, A. Spannenberg and J. Heinicke, *J. Organomet. Chem.*, 2002, **646**, 113–124; (*f*) M. Ghalib, P. G. Jones, S. Lysenko and J. W. Heinicke, *Organometallics*, 2014, **33**, 804–816; (*g*) B. R. Aluri, M. K. Kindermann, P. G. , I. Dix and J. W. Heinicke, *Inorg. Chem.*, 2008, **47**, 6900–6912; (*h*) B. R. Aluri, K. Shah, N. Gupta, O. S. Fomina, D. G. Yakhvarov, M. Ghalib, P. G. Jones, C. Schulzke and J. W. Heinicke, *Eur. J. Inorg. Chem.*, 2014, **2014**, 5958–5968.
56 S. Wu, A. L. Rheingold, J. A. Golen, A. B. Grimm and J. D. Protasiewicz, *Eur. J. Inorg. Chem.*, 2016, **2016**, 768–773.
57 (*a*) J. A. W. Sklorz, S. Hoof, N. Rades, N. De Rycke, L. Könczöl, D. Szieberth, M. Weber, J. Wiecko, L. Nyulaszi, M. Hissler and C. Müller, *Chem.–Eur. J.*, 2015, **21**, 11096–11109; (*b*) S. Ito, K. Koshino and K. Mikami, *Chem.–Asian J.*, 2018, **13**, 830–837; (*c*) R. Schoemaker, K. Schwedtmann, F. Hennersdorf, A. Bauzá, A. Frontera and J. J. Weigand, *J. Org. Chem.*, 2020, **85**, 14420–14434; (*d*) N. Nagahora, S. Goto, T. Inatomi, H. Tokumaru, K. Matsubara, K. Shioji and K. Okuma, *J. Org. Chem.*, 2018, **83**, 6373–6381.
58 (*a*) B. R. Aluri, B. Niaz, M. K. Kindermann, P. G. Jones and J. Heinicke, *Dalton Trans.*, 2011, **40**, 211–224; (*b*) B. R. Aluri, S. Burck, D. Gudat, M. Niemeyer, O. Holloczki, L. Nyulaszi, P. G. Jones and J. Heinicke, *Chem.–Eur. J.*, 2009, **15**, 12263–12272; (*c*) J. Heinicke, N. Gupta, A. Surana, N. Peulecke, B. Witt, K. Steinhauser, R. K. Bansal and P. G. Jones, *Tetrahedron*, 2001, **57**, 9963–9972.
59 G. Becker, W. Massa, O. Mundt, R. E. Schmidt and C. Witthauer, *Z. Anorg. Allg. Chem.*, 1986, **540**, 336–344.
60 V. Vetokhina, M. Kijak, T. M. Lipinska, R. P. Thummel, J. Sepiol, J. Waluk and J. Herbich, *J. Phys. Chem. A*, 2013, **117**, 4898–4906.
61 M. A. Fourati, T. Maris, W. G. Skene, C. G. Bazuin and R. E. Prud'homme, *J. Phys. Chem. B*, 2011, **115**, 12362–12369.
62 Z. Gao, Y. Hao, M. Zheng and Y. Chen, *RSC Adv.*, 2017, **7**, 7604–7609.
63 (*a*) E. L. Mertz, V. A. Tikhomirov and L. I. Krishtalik, *J. Phys. Chem. A*, 1997, **101**, 3433–3442; (*b*) J. Yang, A. Dass, A.-M. M. Rawashdeh, C. Sotiriou-Leventis, M. J. Panzner, D. S. Tyson, J. D. Kinder and N. Leventis, *Chem. Mater.*, 2004, **16**, 3457–3468; (*c*) X. Liu, Z. Xu and J. M. Cole, *J. Phys. Chem. C*, 2013, **117**, 16584–16595; (*d*) P. Horváth, P. Šebej, T. Šolomek and P. Klán, *J. Org. Chem.*, 2015, **80**, 1299–1311; (*e*) N. N. Mohd Yusof Chan, A. Idris, Z. H. Zainal Abidin, H. A. Tajuddin and Z. Abdullah, *RSC Adv.*, 2021, **11**, 13409–13445; (*f*) J. Zhao, S. Ji, Y. Chen, H. Guo and P. Yang, *Phys. Chem. Chem. Phys.*, 2012, **14**, 8803–8817.
64 S. Sarkar, J. D. Protasiewicz and B. D. Dunietz, *J. Phys. Chem. Lett.*, 2018, **9**, 3567–3572.
65 S. Sarkar, H. P. Hendrickson, D. Lee, F. DeVine, J. Jung, E. Geva, J. Kim and B. D. J. Dunietz, *J. Phys. Chem. C*, 2017, **121**, 3771–3777.
66 S. Sarkar, P. Durairaj, J. D. Protasiewicz and B. D. Dunietz, *J. Photochem. Photobiol.*, 2021, 100089.
67 (*a*) S. Bhandari, M. S. Cheung, E. Geva, L. Kronik and B. D. Dunietz, *J. Chem. Theory Comput.*, 2018, **14**, 6287–6294; (*b*) S. Bhandari and B. D. Dunietz, *J. Chem. Theory Comput.*, 2019, **15**, 4305–4311; (*c*) K. Begam, S. Bhandari, B. Maiti and B. D. Dunietz, *J. Chem. Theory Comput.*, 2020, **16**, 3287–3293.
68 Some reviews:(*a*) Kenry, C. Chen and B. Liu, *Nat. Commun.*, 2019, **10**, 2111; (*b*) W. Zhao, Z. He, J. W. Y. Lam, Q. Peng, H. Ma, Z. Shuai, G. Bai, J. Hao and B. Z. Tang, *Chem*, 2016, **1**, 592–602; (*c*) S. Mukherjee and P. Thilagar, *Chem. Commun.*, 2015, **51**, 10988–11003; (*d*) Z. An, C. Zheng, Y. Tao, R. Chen, H. Shi, T. Chen, Z. Wang, H. Li, R. Deng, X. Liu and W. Huang, *Nat. Mater.*, 2015, **14**, 685–690; (*e*) L. Xiao and H. Fu, *Chem.–Eur. J.*, 2019, **25**, 714–723; (*f*) A. D. Nidhankar, Goudappagouda, V. C. Wakchaure and S. S. Babu, *Chem. Sci.*, 2021, **12**, 4216–4236; (*g*) M. Shimizu and T. Sakurai, *ChemPlusChem*, 2021, **86**, 446–459; (*h*) W. Shao and J. Kim, *Acc. Chem. Res.*, 2022, **55**, 1573–1585.